Non-Hermitian Electromagnetic Metasurfaces at Exceptional Points

**Zhipeng Li[1, †], Guangtao Cao[1, 2, †], Chenhui Li[1], Shaohua Dong[1],
Yan Deng[1], Xinke Liu[2], John S. Ho[1], and Cheng-Wei Qiu[1, *]**

(*Invited Review*)

Abstract—Exceptional points are spectral singularities in non-Hermitian systems at which two or more eigenvalues and their corresponding eigenvectors simultaneously coalesce. Originating from quantum theory, exceptional points have attracted significant attention in optics and photonics because their emergence in systems with nonconservative gain and loss elements can give rise to many counterintuitive phenomena. Metasurfaces — two-dimensional artificial electromagnetic materials structured at the subwavelength scale — can provide a versatile platform for exploring such non-Hermitian phenomena through the addition of dissipation and amplification within their unit cells. These concepts enable a wide range of exotic phenomena, including unidirectional propagation, adiabatic mode conversion, and ultrasensitive measurements, which can be harnessed for technological applications. In this article, we review the recent advances in exceptional-point and non-Hermitian metasurfaces. We introduce the basic theory of exceptional point and non-Hermiticity in metasurfaces, highlight important achievements and applications, and discuss the future opportunities of non-Hermitian metasurfaces from basic science to emerging technologies.

1. INTRODUCTION

Closed and conservative systems in quantum theory are required to exhibit real eigenvalues and orthogonal eigenstates described by Hermitian Hamiltonians. In contrast, open and nonconservative systems are associated with non-Hermitian Hamiltonians with complex eigenvalues and non-orthogonal eigenstates [1]. Non-Hermitian systems can therefore exhibit special degeneracies at which two or more eigenvalues and underlying eigenvectors coalesce — called exceptional points (EPs) — which have no counterpart in Hermitian systems [2]. EPs are associated with sharp phase transitions in the eigenvalue spectrum that can dramatically alter the response of the system. Among non-Hermitian systems, the most widely studied case is parity-time (PT)-symmetric system [3] in which the non-Hermitian Hamiltonian $\hat{H}$ satisfies the commutative law $\hat{H}\hat{P}\hat{T} = \hat{P}\hat{T}\hat{H}$, where the parity operator $\hat{P}$ represents the coordinate reverse by mirror reflection, and the time operator $\hat{T}$ acts as complex conjugation [4]. Counterintuitively, PT symmetric systems can support entirely real eigenvalue spectra [1] despite having non-Hermitian Hamiltonians. An abrupt phase transition appears when a non-Hermitian operator crosses an EP: The spectrum ceases to be real (exact-PT phase) and starts to be complex (broken-PT phase), i.e., the Hamiltonian and the PT operator no longer share the common eigenfunctions.

While experimental realization of EP in a quantum systems is challenging, optical and photonic systems have recently provided fertile ground for the investigation of non-Hermitian physics because of the ease by which nonconservative elements for optical gain and loss can be controllably

introduced [5]. Owing to the formal equivalence between the Schrödinger wave equation and the paraxial electromagnetic wave equation [6], a non-Hermitian Hamiltonian can be achieved by spatially modulating dissipation and amplification in wide range of optical and photonic systems, including coupled microcavities, fibre loops, and waveguides [7–9]. For example, a PT symmetric system can be implemented using two coupled microtoroidal whispering-gallery-mode resonators in which optical gain is achieved in an active resonator by ion dopants, and the other resonator is intrinsically lossy [10]. This system exhibits a clear phase transition from the broken-PT phase to the exact-PT phase where the imaginary eigenfrequencies degenerate, and the real parts bifurcate. Non-reciprocal light transmission can also be observed by optical nonlinearity in the broken-PT phase due to the strong field localization in the active resonator [11].

Metasurfaces are artificial two-dimensional electromagnetic materials consisting of periodic subwavelength unit-cells which can achieve unusual electric and magnetic responses not available with natural materials [12]. By engineering the geometry and composition of individual unit-cells, metasurfaces can be designed to manipulate light by abruptly changing its amplitude, phase, and polarization [13]. They have been used to engineer ultrathin interfaces with extraordinary properties including anomalous refraction/reflection, polarization control, vortex beam generation, and subwavelength focusing [14–18] for fascinating applications such as invisible cloaks, prefect absorbers, and holograms [19–23]. Due to their subwavelength periodicity, metasurfaces can be characterized by effective permittivity and permeability that can be designed arbitrarily from negative values to positive values. For example, the idea of simultaneously negative values of permittivity and permeability has been proposed and theoretically shown that negative index material has unique properties to make a perfect lens [24]. Negative index materials have been experimentally constructed by metallic thin wires and split ring resonators that provide negative permittivity and negative permeability, respectively [25]. Beyond the real-valued permittivity and permeability, non-Hermiticity further extends the design of metasurface to the entire space of complex permittivity and permeability, focusing on the delicate interplay between the real and imaginary parts of refractive index, i.e., gain and loss [26]. Non-Hermiticity can therefore provide the means to leverage gain/loss and engineer metasurfaces with expanded functionalities.

In this article, we review the recent advances in exceptional-point and non-Hermitian metasurfaces. We first introduce the basic theory and fundamental concepts of exceptional point, non-Hermiticity, and their connection with metasurfaces. We then highlight the important achievements and applications ranging from unidirectional propagation, polarization control, diffraction control, ultrasensitive sensing and biosensors, imaging, to surface waves. Finally, we discuss the future opportunities of non-Hermitian metasurfaces from basic science to emerging technologies.

2. THEORY

2.1. Non-Hermiticity and Exceptional Point

We start from the one-dimensional single-particle Schrödinger equation:

$$i\hbar\frac{\partial\Psi}{\partial t} = -\frac{\hbar^2}{2m}\frac{\partial^2\Psi}{\partial x^2} + V(x)\Psi \tag{1}$$

where Ψ is the wave function, $\hbar$ the reduced Plank constant, m the single-particle mass, and $V(x)$ the potential. The Hamiltonian $H = -\frac{\hbar^2}{2m}\frac{\partial^2}{\partial x^2} + V(x)$ describes the total energy of a system. In a conservative system or an isolated system with no energy exchange with ambience. $V(x)$ is real, and the Hamiltonian always satisfies $H = H^*$, where $*$ represents Hermitian conjugate, resulting in real eigenenergy and unitary time evolution. However, in an open system, the potential $V(x)$ becomes a complex function because of the coupling with the environment, consequently leading to a non-Hermitian Hamiltonian.

In 1998, Bender and Boettcher presented a special case [1] that, if a non-Hermitian Hamiltonian commutes parity-time operator $[H, PT] = 0$ where the parity operator P reverses the spatial coordinate position $(\hat{p} \rightarrow -\hat{p}, \hat{x} \rightarrow -\hat{x}, i \rightarrow i)$ and the time-reversal operator T reverses the time evolution $(\hat{p} \rightarrow -\hat{p}, \hat{x} \rightarrow \hat{x}, i \rightarrow -i)$ [27], the system can counterintuitively support entirely real eigenvalue spectra in exact-PT phase, and the eigenspectra become complex if the PT symmetry is broken [28]. In

the exact-PT phase, the wave functions exhibit a symmetric probability distribution. In the broken-PT phase, the complex-conjugate eigenvalues result in the asymmetry probability distribution. An EP can be located where the system transits from exact-PT phase to broken-PT phase — the eigenvalues of the Hamiltonian rapidly degenerate into one (Fig. 1(a)).
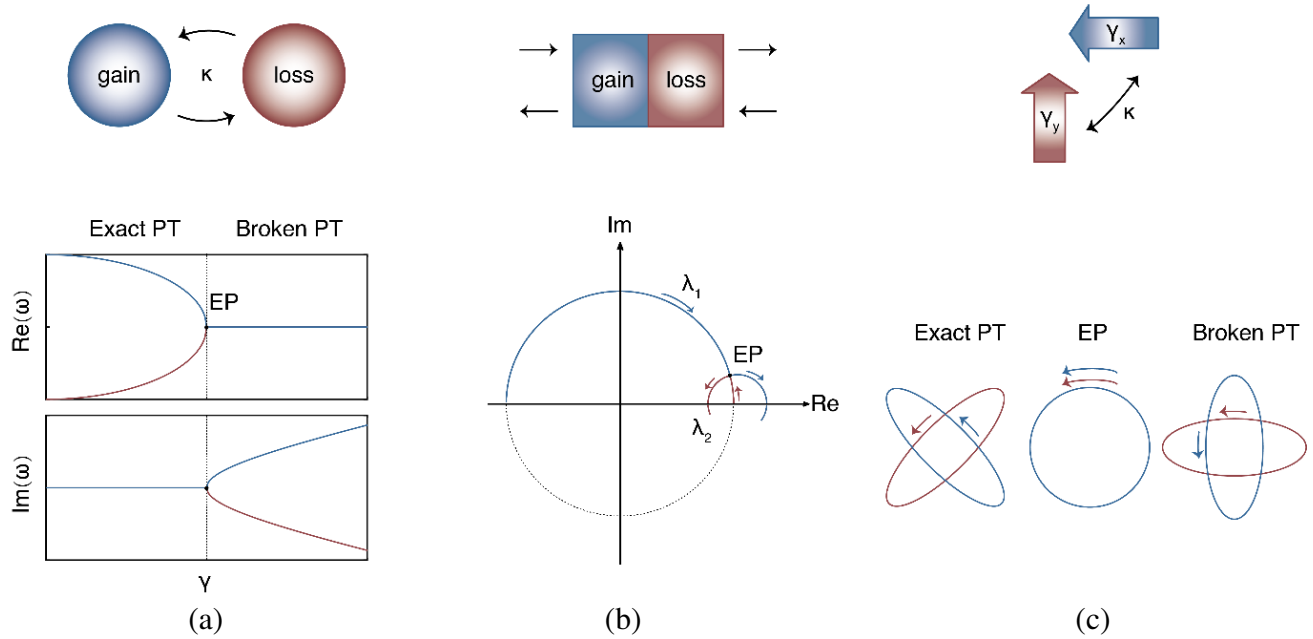

Figure 1. Theoretical models of non-Hermitian metasurfaces. (a) A PT-symmetric two-level system of two coupled resonators with gain (blue) and loss (red), and the corresponding eigenvalues versus the gain-loss contrast γ. The phase transition from exact-PT phase to broken-PT phase happens at the EP. (b) A two-port system of balanced gain (blue) and loss (red), and the corresponding eigenvalues versus the normalized resistance parameter k. A spontaneous splitting happens at $k = 0.5$. (c) Two perpendicular dipoles with different dissipation losses, and the corresponding eigenpolarizations versus the coupling κ. At the EP, the eigenpolarizations are collapse to a single left circularly polarized state.

2.2. Exceptional Point in Electromagnetics

In the paraxial limit, the slowly varying envelope along the paraxial direction z can be described by the Schrödinger-like Equation [29]:

$$i\frac{\partial E}{\partial z} = -\frac{1}{2k_0}\frac{\partial^2 E}{\partial x^2} + k_0 n\left(x\right) E \tag{2}$$

where E is the transverse electric field profile, k_0 the wavenumber in free space, and $n(x) = n_R(x) + in_I(x)$ the complex refractive index distribution in the non-Hermitian electromagnetic system. The real-part refractive index represents the dispersion, and the imaginary part denotes the gain or loss of the energy. The equivalent optical Hamiltonian is $H = -\frac{1}{2k_0}\frac{\partial^2}{\partial x^2} + k_0 n(x)$, and the optical potential is $V(x) = k_0 n(x)$. In analogy to quantum theory, PT symmetry can be realized in an optical non-Hermitian system when the optical potential satisfies $n(x) = n^*(-x)$. To be specific, the real part must be an even function $n_R(x) = n_R(-x)$, and the imaginary part needs to be odd $n_I(x) = -n_I(-x)$, i.e., balanced gain and loss [30].

Alternatively, a two-level coupled electromagnetic system with gain and loss resonators can be described by a Hamiltonian derived from the standard coupled mode equation [31]:

$$H = \begin{pmatrix} \omega_1 + ig & \kappa \\ \kappa & \omega_2 - i\gamma \end{pmatrix} \tag{3}$$

where $\omega_{1,2}$ are the resonance frequencies; κ is the coupling coefficient; g is the gain of one resonator; and γ is the loss of the other one. In a particular case of balanced gain and loss ($g = \gamma$), the system is PT-symmetric under exact resonance ($\omega_1 = \omega_2 = \omega_0$), and the eigenvalues of the Hamiltonian are:

$$\omega_\pm = \omega_0 \pm \sqrt{\kappa^2 - \gamma^2} \tag{4}$$

Above equation shows the exact-PT phase and broken-PT phase (Fig. 1(a)). When $\gamma < \kappa$, the eigenvalues are purely real. The associated eigenstates satisfy PT symmetry, and the energy of each resonator keeps constant due to vanished imaginary parts. When $\gamma > \kappa$, the eigenvalues are conjugate pairs with nonzero imaginary parts, leading to an asymmetric eigenstates distribution that is strongly amplified in the gain resonator and exponential decays in the loss side. Specially, at an EP ($\gamma = \kappa$), the eigenvalues coalesce to a single value $\omega = \omega_0$, corresponding to degeneracy of the non-Hermitian eigenstates.

In practical applications, the inconvenient implementation of optical amplification in PT-symmetric system leads to the proposal of open PT symmetry in a two-level system with two unequal losses. In this case, the Hamiltonian can be divided into two parts: a PT-Hamiltonian and a system attenuation having no influence on the phase transition:

$$H = H_{PT} + H_L = \begin{pmatrix} \omega_0 - i\gamma_{diff} & \kappa \\ \kappa & \omega_0 + i\gamma_{diff} \end{pmatrix} + \begin{pmatrix} -i\gamma_{ave} & 0 \\ 0 & -i\gamma_{ave} \end{pmatrix} \tag{5}$$

where $\gamma_{ave} = (\gamma_1 + \gamma_2)/2$ is the average loss of the two components, and $\gamma_{diff} = (\gamma_1 - \gamma_2)/2$ is the contrast of the two losses. Thus, a "virtual gain" can be achieved to combat the loss [32]. We can still define exact-PT phase and broken-PT phase by H_{PT}, although H is offset by a global loss H_L with eigenvalues that are no longer real [26].

2.3. Non-Hermitian Metasurfaces

A two-port metasurface can be described by a scattering matrix (Fig. 1(b)) that can be obtained by transmission matrix [33], impedance matrix [34], or admittance matrix [35], and sometimes combine with the coupled mode equations [36]. In metasurfaces satisfying PT symmetry, the scattering matrix of an active two-port system with balanced gain and loss has the form:

$$S = \begin{pmatrix} t_1 & r_1 \\ r_2 & t_2 \end{pmatrix} \tag{6}$$

where $t_{1,2}$ are the reciprocal transmission coefficients ($t_1 = t_2 = t$), and $r_{1,2}$ are the reflection coefficients of the first and second ports, respectively. Although we only consider the active condition in the following analysis, the passive scattering matrix has a similar PT-phase transition by separating a trivial uniform damping as shown in Eq. (5). Based on the analogy between the Hamiltonian matrix and scattering matrix, the PT-phase transition of this system can also be observed according to its eigenvalues:

$$\lambda_\pm = t \pm \sqrt{r_1 r_2} \tag{7}$$

Similar to Eq. (4), two configurations of the eigenvalues (from unimodular to non-unimodular) feature the transition between exact-PT phase and broken-PT phase (Fig. 1(b)). In the exact-PT phase, the gain/loss contrast is weak, and λ is unimodular. Similar to a PT-symmetric system with constant energy indicated by real eigenvalues, here the unimodular $\lambda_\pm$ also describes power conservation in a non-conserved system with a unitary scattering matrix. In addition, a generalized conservation law [37] can also be obtained by calculating the power of either gain or loss region $P = T + \sqrt{R_1 R_2}$, where $T = |t|^2$ is the transmittance, and $R_{1,2} = |r_{1,2}|^2$ is the reflectance. It can be proved that $P = 1$ is valid for both eigenstates in agreement with the unimodular λ in exact-PT phase. In the broken-PT phase, λ is no longer unimodular and can be divided into gain and loss eigenstates with $P \neq 1$. Superunitary eigenvalue leads to a state that localizes more on the gain resonator representing amplification, while subunitary eigenvalue stands for damping in the loss resonator.

At an EP where PT-symmetry is spontaneously broken, the fascinating properties of scattering matrices have been studied extensively, such as unidirectional reflectionless transition. For example, a

metasurface consisting of two parallel sub-elements with balanced gain and loss [38] can be described by a scattering matrix:

$$S = \begin{pmatrix} t & r_1 \\ r_2 & t \end{pmatrix} = \begin{pmatrix} \dfrac{1}{e^{jx} - \dfrac{j\sin(x)}{2k^2}} & \dfrac{(1+2k)\sin(x)}{-\sin(x) - 2jk^2 e^{jx}} \\ \dfrac{(1-2k)\sin(x)}{-\sin(x) - 2jk^2 e^{jx}} & \dfrac{1}{e^{jx} - \dfrac{j\sin(x)}{2k^2}} \end{pmatrix} \tag{8}$$

where k is the normalized resistance parameter $\{k \in R : k \geq 0\}$ corresponding to the surface impedance of the gain and loss components $Z_{g,l} = \pm kZ_0$, $Z_0 = \sqrt{\frac{\mu_0}{\varepsilon_0}}$, and x is the electrical length between the two resonators. Characterizing the eigenvalues with dynamic κ and fixeing x in the polar diagram (Fig. 1(b)), we can observe a spontaneous splitting at $k = 0.5$ where $r_2 = 0$, $t = e^{jx}$. Therefore, the transmission is flux-conserving from both ports but the reflection from port two vanishes in this condition, manifesting unidirectional reflectionless transmission.

Non-Hermiticity has also shown remarkable performance in manipulating circularly polarized wave using, for example, anisotropic metasurfaces with mirror symmetry [39]. The feature of polarization control could also be combined with nonreciprocity to achieve unidirectional polarization conversion [40, 41]. As shown in Fig. 1(c), two resonators in a unit-cell are generally considered as perpendicular dipoles with different dissipation losses γ_x^d, γ_y^d due to their different geometries or constituent materials. The distance-dependent coupling κ between the resonators is a real factor since the two sets of dipoles radiate into orthogonal polarization states preventing radiative coupling. An equivalent Hamiltonian with balanced gain and loss can be written as:

$$H = \begin{pmatrix} -i\dfrac{\gamma_y^d - \gamma_x^d}{2} & \kappa \\ \kappa & i\dfrac{\gamma_y^d - \gamma_x^d}{2} \end{pmatrix} \tag{9}$$

The PT-phase transition (Fig. 1(c)) is determined by a parameter $\Delta = \sqrt{4\kappa^2 - (\gamma_x^d - \gamma_y^d)^2}$. In a strong coupling $2\kappa > |\gamma_x^d - \gamma_y^d|$ corresponding to the exact-PT phase, the eigenpolarizations of the metasurface are given by $(\hat{x} \pm e^{\pm i\theta}\hat{y})$ with $\theta = \sin^{-1}[(\gamma_x^d - \gamma_y^d)/2\kappa]$. The polarization states show two corotating ellipses (Fig. 1(c)) with major axes along $\pm 45°$. EP occurs when the dipoles separate from each other with $2\kappa = |\gamma_x^d - \gamma_y^d|$, where the eigenpolarizations are collapsed to a single left or right circularly polarized state determined by the sign of $\delta = \gamma_x^d - \gamma_y^d$. Further increasing the distance leads to broken PT-symmetry when $2\kappa < |\gamma_x^d - \gamma_y^d|$. The eigenpolarizations become two ellipses with major axes along $0°$ and $90°$ with the form of $(\hat{x} \mp ie^{\theta}\hat{y})$ where $\theta = \cosh^{-1}[(\gamma_x^d - \gamma_y^d)/2\kappa]$.

3. APPLICATIONS

3.1. Unidirectional Propagation

Unidirectional propagation, an intriguing phenomenon in a two-port scattering system with different transmission or reflection at the two ends, has raised tremendous attention in designing photonic devices such as modulators, imaging devices, and switches [42]. In recent years, theoretical and experimental explorations of EPs have been extensively reported to achieve unidirectional propagation in non-Hermitian scattering systems including gratings [43, 44], metamaterials [36], waveguides [45], multilayer structures [46], and waveguide-cavity structures [7, 47, 48]. For example, Chen and Jung proposed a PT-symmetric metasurface to realize the unidirectional reflectionless propagation of terahertz waves [38]. The metasurface is composed of optically pumped graphene and a resistive metallic filament separated by dielectric or gas gap, as shown in Fig. 2(a). In the terahertz regime, the graphene metasurface with optical pumping displays a negative surface resistance owing to cascaded optical-photon emissions
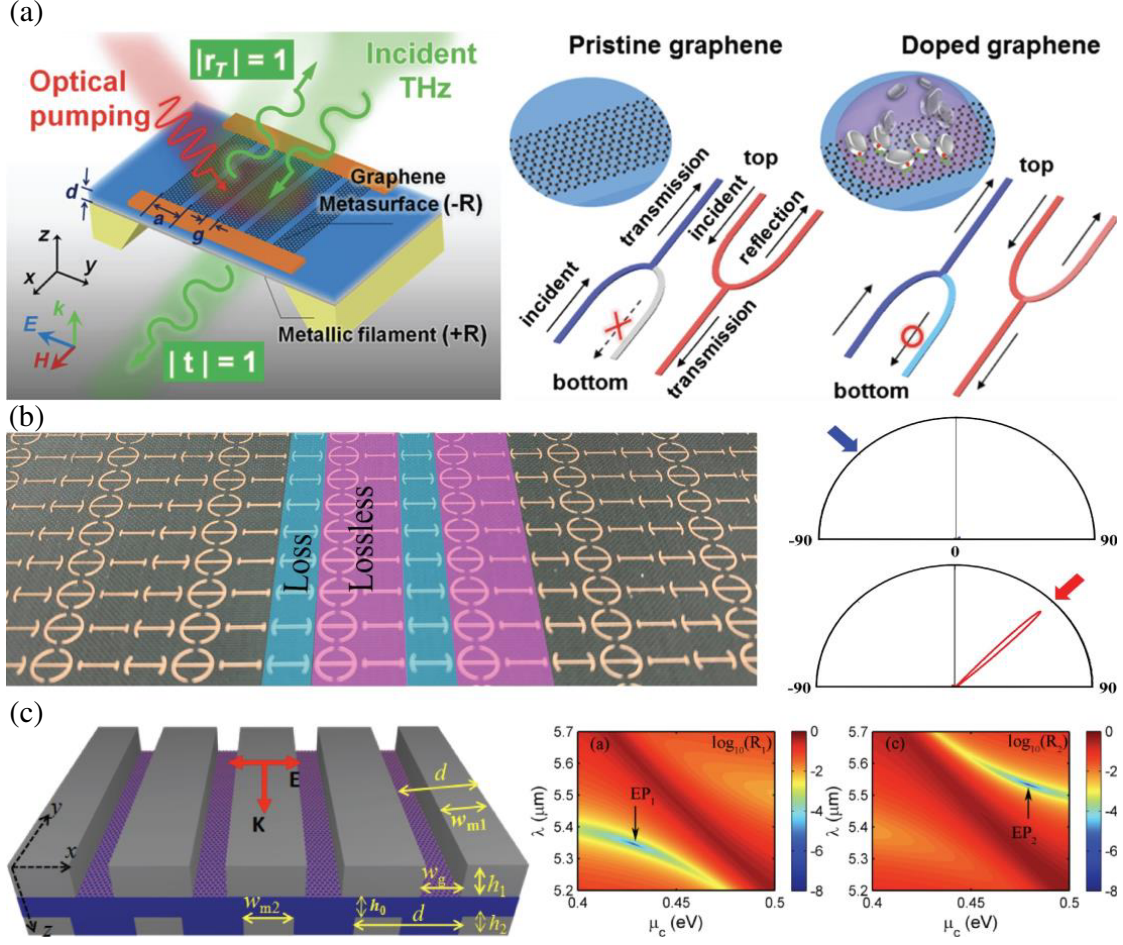
Figure 2. Unidirectional retro-reflection generating based on non-Hermitian metasurfaces. (a) Left panel: Schematic of PT symmetric system composed of graphene metasurface and metallic filament. Right panel: Diagram of transmission and reflection of the terahertz wave incident from the top and bottom of the PT symmetric system with pristine and doped graphene metasurface. Reproduced with permission [38]. (b) Left panel: Picture of fabricated experimental sample composed of lossless and loss regions. Right panel: Far-field scattering features of the metasurface as a function of detection angle for electromagnetic wave incident from the left and right ports. Reproduced with permission [54]. (c) Left panel: Schematic of hybrid structure composed of silver gratings and graphene ribbons. Right panel: Reflection spectra $R1$ and $R2$ versus graphene μ_c and incident wavelength λ. Reproduced with permission [59].

and population inversion, which performs as gain thin sheet and could balance the loss introduced by the absorbing metallic filament. Thanks to the unusual properties around the EP (see Eq. (8)), the judiciously constructed graphene metasurface enables unidirectional reflectionless propagation, which could be effectively modulated by dynamic conductivity that is sensitive to n- or p-type surface adsorbates in graphene. This PT-symmetric metasurface operated at the EP also shows the potential to be used as chemical or biological sensors with enhanced sensitivity.

Gain-mediated non-Hermitian metasurfaces needs careful tuning of system gain to balance the loss, which causes complexity and inefficiency in the design and application of non-Hermitian metasurfaces [3, 49]. Non-Hermitian metasurfaces with two unequal losses have been proposed to overcome this challenge [50, 51]. Although the losses such as intrinsic loss and radiation loss in photonic devices are usually minimized in optics and photonics to enhance efficiency, EPs in non-Hermitian systems can pave a new way in converting the undesired losses into advantages for expanding

the functionalities of photonic devices [52, 53]. For example, Dong et al. investigated a loss-assisted non-Hermitian metasurface operating at an EP to show unidirectional retro-reflection [54]. This non-Hermitian metasurface is composed of tri-meta-atom supercells (H-shape metal rings) with balanced lossy and lossless interlaced regions, in which the loss is introduced by leaky radiation due to the slits with adjustable width in the metal base, as depicted in Fig. 2(b). They illustrated the evolution of the eigenvalues $E_\pm$ of scattering matrix for the electromagnetic metasurface. An EP in parametric space appears as the two eigenvalues coalesce. This metasurface has shown a distinguished nonreciprocal scattering feature: high-efficient reflection under an incidence from the right and fully suppressed reflection from the left. In addition, the far-field scattering features (Fig. 2(b)) of the metasurface prove the totally suppressed and highly efficient retro-reflection (4% from left port and 90% from right port at 11.8 GHz), which provides a new perspective for designing an asymmetric optical system for wave manipulation. Unidirectional reflectionless propagation has also been achieved in a non-Hermitian metasurface consisting of two silver ring resonators coupled in the far field [33]. This metasurface shows a bilateral unidirectional reflectionless propagation that is insensitive to the incident angle ($\sim 25°$) and independent of polarizations.

Unidirectional propagation in above non-Hermitian metasurfaces requires accurate location of EPs, which needs careful tuning of the system parameters such as intercellular coupling or loss. Accurate and efficient locating of EP could be accomplished by tracking the Fano-resonant-type abrupt transmission/reflection transitions when the system is encircling the EP in parameter space. Fano resonance describes a sharp asymmetric lineshape with abrupt intensity changes and extreme singularities generated from the interference of two coupled resonators with a continuum state and a discrete state [55–58]. For example, a Fano-resonant graphene metasurface has been proposed [59] to show a sharp reflection changes when the system parameters are varied to encircle the EP. The metasurface consists of a double-layer metallic grating structure and single-layer graphene nanoribbons, in which the valleys of Fano-type reflection can be tuned by chemical potential of graphene. As schematically shown in Fig. 2(c), the reflection spectra $R1$ and $R2$, corresponding to the light impinged from top and bottom, are clearly different. The abruptness of this reflection changes can be maximized near an EP (zero reflection point), which could become an alternative and efficient method to locate EP instead of seeking the bifurcation of real eigenfrequencies or the cross of magnitude and phase. The topological structure of EP is studied in the parameter space of incident wavelength and chemical potential of graphene, showing a self-inserting Riemann surface with crossing and anti-crossing properties. This non-Hermitian metasurface has also shown a unidirectional reflectionless propagation at the EP that is sensitive to the chemical potential of graphene.

3.2. Polarization Control

Metasurfaces have facilitated an interesting platform to explore the EPs in polarization space benefiting from the anisotropic engineering of metasurfaces that support large refractive index contrast between orthogonal polarizations. Polarization determines the interaction between electromagnetic wave and matters, which has attracted tremendous attentions in almost every area of science ranging from optical communication to biomedical sensing [60]. Compared with the traditional devices, the polarizers based on metasurfaces are of vital interest owning to their miniaturization and tunability [56, 61–63]. Non-Hermiticity further offers a new degree of freedom to design chiral metasurface with gain/loss manipulation, leading to intriguing phenomena such as direction-dependent polarization converting and superchiral field generation.

Non-Hermitian metasurfaces for polarization control, usually constructed by coupled split-ring resonators, render the PT-symmetric phase transition effect by modulating the system parameters such as the resonance frequencies and dissipation loss rates of resonators, and their intercellular coupling strength [34, 64]. For example, Lawrence et al. proposed a loss-assisted non-Hermitian metasurface with PT-phase transition in polarization space [39]. This metasurface is mirror symmetric, consisting of orthogonally oriented split-ring resonators with different Ohmic losses determined by different materials, as shown in Fig. 3(a). Spontaneous PT-symmetry breaking is achieved by the variation of coupling strength through adjusting the distance of intercellular meta-atoms, which gives rise to a sudden 45° rotation of eigenpolarization ellipses. When the EP is reached, the two eigenpolarization states merge into a circularly polarized state despite the lack of rotational symmetry of the non-Hermitian
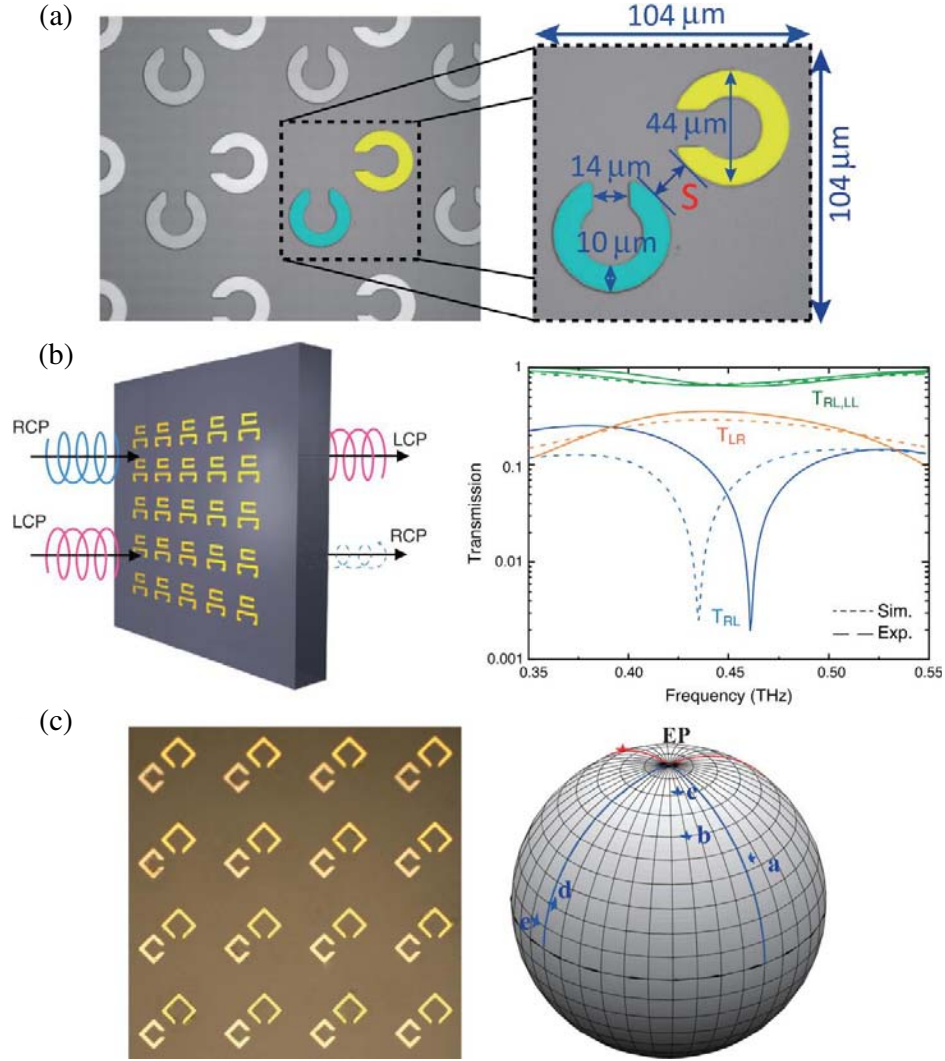
Figure 3. EP in polarization space with non-Hermitian metasurfaces. (a) Picture of metasurface consists of silver and lead split-ring resonators on silicon substrate. Reproduced with permission [39]. (b) Illustration of asymmetric transmission of circularly polarized incident waves. Reproduced with permission [65]. (c) Left panel: Schematic of hybridized metasurface made of Au and type II superconductor NbN. Right panel: Eigen-polarization states plotted on the Poincare sphere with the temperature varying from 2 to 13 K. Reproduced with permission [34].

metasurface. Park et al. also designed a non-Hermitian metasurface with a similar architecture to explore the topology of EP encirclement in the parameter space of coupling strength and incident wavelength [65]. The topology of the self-intersecting Riemann surface that is unique to non-Hermitian systems [9, 66, 67] has been observed by the behavior of level crossing in the magnitude and phase of the eigenvalues. Due to this unique topology, the pair of polarization states (represented by ellipticity angle and orientation angle) under one full loop encirclement around the EP do not return to the original values but rather are swapped with each other and accumulate a geometric phase of π on one of the states. Asymmetric transmission of circularly polarized light — the smaller conversion from LCP to RCP than that of inverse conversion — is also observed near the EP, as illustrated in Fig. 3(b). Other phenomena stemming from EP are also observable, such as enhanced sensitivity of phase dispersion and abrupt phase flip in the cross-polarization transmission.

Non-Hermitian metasurfaces in polarization space can also be used to generate superchiral fields

that have great potentials to detect chirality. For example, a chiral EP with homogeneous superchiral fields has been demonstrated in a non-Hermitian metasurface-like photonic crystal slab composed of an array of cylindrical holes. By tuning the diameter and thickness of the holes and breaking the up-down symmetry, a pair of TM- and TE-like modes can be spectrally close to each other and become coupled. The coupling strength and radiation loss of this pair of orthogonal polarization modes can be further tuned by the system geometric parameters, leading to a "vector" EP [68]. Due to direction-dependent excitation of orthogonal polarization modes, the uniform superchiral fields can be generated at the EP by two incident beams with opposite directions. In addition, the chirality of EPs has also been shown in non-Hermitian chiral metasurfaces composed of periodic arrays of orthogonally oriented graphene strips [69] or plasmonic resonators [70]. For example, the chiral EPs emerge by tuning the geometric parameters of graphene strips and incident wavelengths, and their chirality is opposite and relates to completely LCP or RCP output [69]. The chirality of the EPs also shows a reversible feature when the light is incident from the opposite direction of the metasurface.

To uncover the dynamics of EP encirclement in polarization space, a series of metasurface samples with different geometric parameters need to be fabricated to control the coupling strength near the EP [34, 71], which make it difficult to fine-tune parameters and may induce undesired perturbations due to fabrication errors. To solve this problem, the wavelength and angle of incident light have been selected as the parameter space to continuously control the phase transition around EP and observe its topological structure [65, 71]. Reconfigurable metasurfaces have also been proposed to analyze the evolution of EP in polarization space to avoid the requirement of a great number of experimental samples. The reconfigurability has been achieved in metal-graphene and metal-NbN hybridized metasurfaces with continuously tunable loss thanks to stimuli-controlled Fermi level of graphene and temperature-dependent conductivity in NbN [34, 72]. For example, Fig. 3(c) shows that the hybridized metasurface is made of Au and type II superconductor NbN [34]. Based on the measured amplitude and phase, the eigen-polarization states are plotted on the Poincare sphere. It is demonstrated that the eigen-polarization states approach and deviate from the north pole of Poincare sphere, indicating the location of the PT-symmetry transition point, i.e., EP, as the temperature varies from 2 to 13 K. When the temperature is around 9 K, the eigen-polarization state is close to the north pole of Poincare sphere. Therefore, tuning the temperature, which could dynamically change the dissipation loss of NbN, puts forward a feasible way to exhibit the dynamic process of PT-symmetry transition. The topological structure of EP has also been studied in a non-Hermitian metasurface composed of a pair of I-shaped resonators as unit cell and in parameter space of incident angle and frequency [66].

3.3. Diffraction Control

Metasurfaces impose discontinuous phase shifts at the boundaries of subwavelength units due to resonant excitation of effective wavevector, leading to anomalous reflection or diffraction fields with arbitrary wavefront [73]. The materials used in metasurfaces with Hermitian settings, such as metal or dielectric materials, however, induce significant energy dissipation and thus reduce the efficiency of metadevices [74]. Non-Hermitian metasurfaces with engineered gain and loss can offer a solution to enhance device efficiency and may bring new controls of scattering fields. For example, a flexible PT-symmetric metasurface has been proposed for diffraction control [75]. The unit cell of metasurface is composed of near-field-coupled scatters on a flexible substrate and in honeycomb arrangement (Fig. 4(a)). A passive PT symmetry is based on the near-field interaction between the lossy and lossless elements. This metasurface can generate scattering fields with six distinct diffraction orders under visible illumination. In broken PT-symmetry phase, the diffraction fields with six orders are lopsided with an extinction ratio of −8 dB, showing an asymmetric light transport.

The integration of PT-symmetric phase and geometric phase in a single non-Hermitian metasurface has also been proposed in theory for polarization-sensitive manipulation of diffraction fields [76]. The hybrid metasurface is firstly designed by a rectangular hole array in a conductive slab, in which geometric phase is implemented by the spatial rotation of the unit cell, and the refractive field with first diffraction order and opposite polarization is observed. PT-symmetric phase is then imprinted into the geometric-phase metasurface by attaching a proper gain/loss into each unit cell, which leads to two new diffraction orders insensitive to incidence polarization. The hybrid phase is thus polarization sensitive and may enable new metadevices to manipulate optical fields with polarization dependence (Fig. 4(b)).
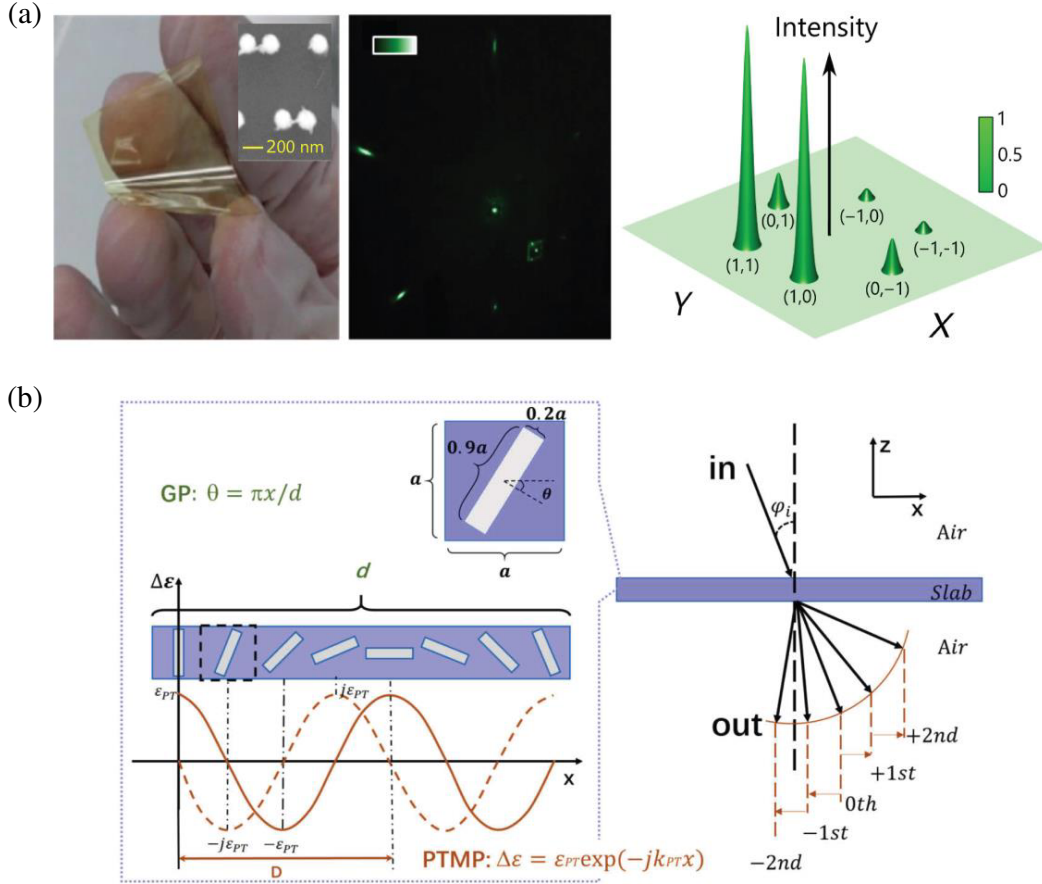
Figure 4. Non-Hermitian metasurfaces for diffraction control. (a) Left panel: Photo of flexible metasurface and SEM image of the irregular hexagonal pattern. Middle panel: Far-field emission under PT-symmetric condition. Right panel: Power-diffraction efficiencies for PT-symmetric configuration. Reproduced with permission [75]. (b) Left panel: Schematic of the metasurface structure. Geometric phase is achieved by rotated holes and a PT-symmetric perturbation with a period of $4a$ is imposed on the medium filling the hole array. Right panel: Diffraction fields with different diffraction orders. Reproduced with permission [76].

3.4. Ultrasensitive Sensing and Biosensors

Enhanced sensitivity is one of the most striking properties in PT symmetry systems [77]. For a PT symmetric system operating at N-order EP where N eigenvalues and the associated eigenstates simultaneously coalesce, an external perturbation forces the system to move from an EP to exact-PT phase, contributing to an enhanced frequency splitting that scales with Nth-root of perturbation strength ε. This nonlinear splitting to a sufficiently small perturbation, defined as the sensitivity, has proven to be larger than the linear splitting in a system with conventional degeneracies known as diabolic points [77] as shown in Fig. 5(a). In optics, enhanced sensitivity by second-order EP has been demonstrated in an optical microcavity supporting two travelling modes [78]. Square-root topology was observed when a nanoparticle enters the mode volume as external perturbation, shifting the system away from an EP and leading to a frequency splitting proportional to $\varepsilon^{1/2}$. A third-order EP in a ternary coupled microring laser system has exhibited higher sensitivity than that of second-order EP. Enhanced sensitivity has also been demonstrated in wireless circuits locked to an EP, which have been used for sensitive physiological state monitoring [79].

EP-enhanced sensitivity has been theoretically illustrated in a non-Hermitian metasurface composed of passive PT-symmetric resonators [80]. The resonators are split-ring bilayer structures with
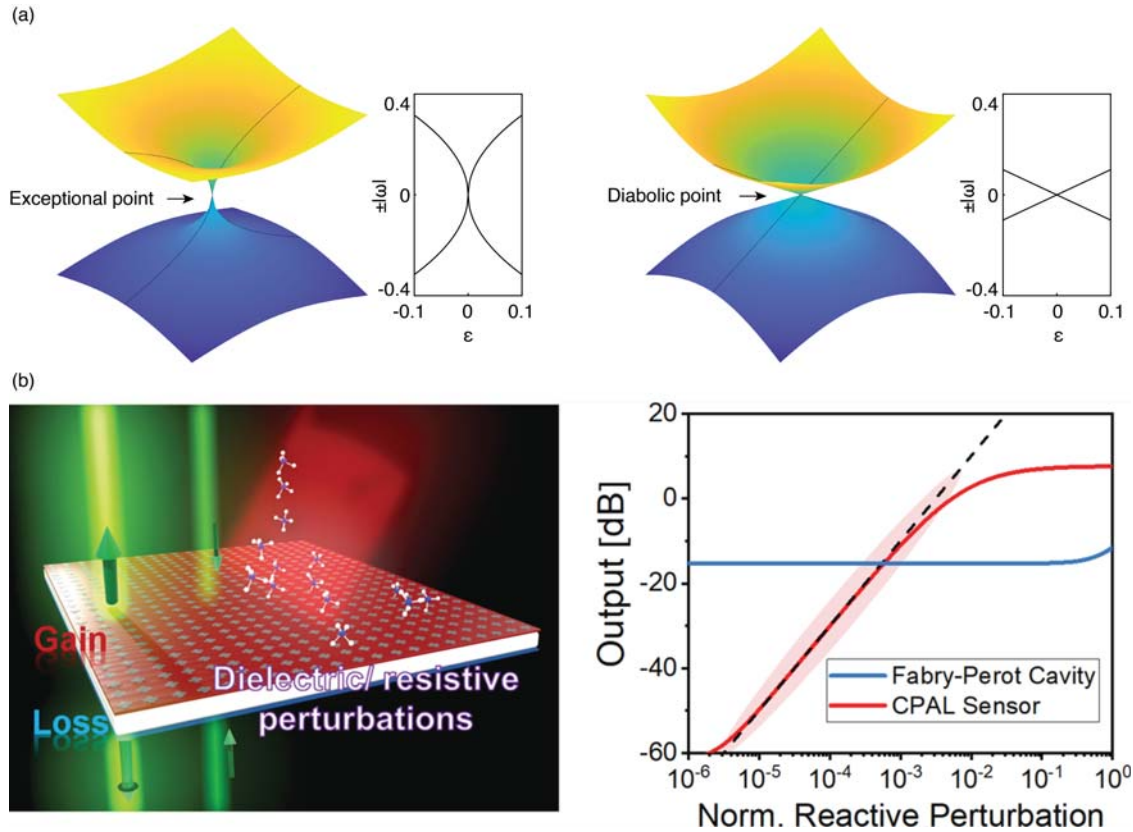
Figure 5. Non-Hermitian metasurfaces for ultrasensitive sensing and biosensors. (a) The comparison of nonlinear exception-point sensing (left panel) and linear diabolic-point sensing (right panel). Reproduced with permission [78]. (b) Left panel: Schematic of a PT-symmetric metasurface for molecule detection. Right panel: Demonstration of the metasurface operating at a CPAL point with an enhanced sensitivity compared to the sensing using a Fabry-Perot cavity. Reproduced with permission [83].

orthogonally orientated gaps. The bilayer structures resonate identically and in terahertz but with high loss contrast induced by different materials (titanium and gold). An EP can be approached by tuning the geometric parameters of coupled resonators when both the eigenfrequencies and eigenvectors coalesce. This EP-sensor is evaluated via a sensitivity defined by eigenfrequency shift per micrometer in thickness and per refractive index unit (RIU). The sensitivity can reach $800\,\mathrm{GHz}\,\mathrm{RUI}^{-1}\,\mathrm{um}^{-1}$ in theory, which is an order of magnitude higher than conventional terahertz biosensors in Hermitian settings [81, 82]. In addition to exceptional sensitivity based on intensity or resonant frequency changes, phase changes or polarization rotations can also be monitored for ultrasensitive sensing. For example, a metal-graphene hybrid metasurface with tunable asymmetric loss has been proposed in terahertz regime [72]. The unit cell consists of two orthogonally oriented split-ring resonators with identical dimensions, and one resonator contains a graphene patch at the gap that can be tuned by changing the conductivity of the graphene. An EP is observed in the parameter space of frequency and dissipation loss where the cross-polarized transmissions are the same. The system experiences an abrupt phase change of π and polarization rotation when crossing this EP, which could be functioned as an ultra-sensitive sensor for surface absorbates such as biomolecules and bacterial while sacrifice the sensing range. Enhanced sensitivity has also been demonstrated in a PT-symmetric metasurface operating at a coherent perfect absorber-laser (CPAL) point [83] (Fig. 5(b)). At a CPAL point, the system's scattering matrix has zero and infinity eigenvalues, corresponding to two system's states: coherent perfect absorber state and lasing state. Under two coherent input waves, a small perturbation of admittance or refractive index can drastically vary the system's output intensity from coherent absorption to lasing, leading to enhanced sensitivity compared to the conventional optic sensors such as Fabry-Perot cavities. An enhancement

factor of 400 has been reported in theory when the absorption is compared at the CPAL point with a passive perfect absorber [84]. However, this high sensitivity may be limited by fabrication error and spontaneous emission noise in practical sensors, which needs further experimental evaluation.

Biomolecule sensing based on EPs has been explored in a passive bilayer metasurface [85]. This metasurface is composed of bilayer plasmonic gold nanorods with spatial symmetry breaking. Based on hybridization of detuned resonances of multilayered dissimilar resonators, the system reaches a critical complex coupling rate between resonator arrays, which enables the simultaneous coalescence of resonances and loss rates with emergence of a plasmonic EP. Enhanced sensitivity of plasmonic EP was presented by sensing of anti-IgG. The resonance splitting around EP follows a square-root topology, which is larger than diabolic-point sensor when the concentration of anti-IgG is small. Further reducing the concentration of anti-IgG, the splitting of diabolic-point sensor does not change further which illustrates the limitation of conventional plasmonic sensors. The sensitivity of plasmonic EP sensor is reported as $4821\,\mathrm{nm}$ per RIU and $15 \times 10^{-12}\,\mathrm{gl}^{-1}$, which has not been reached by previous plasmonic array sensors. The limitation of this plasmonic EP sensor is the low spectrum resolvability due to low quality-factor resonances in the fully passive system. In addition, the sensitivity enhancement in the experiments is not as high as in theory because EP-metasurface sensors require high precision of fabrication [86].

3.5. Imaging

Metamaterials with negative refraction index can realize a perfect lens with imaging properties that do not exist in conventional lenses such as aberration-free and sub-diffraction imaging [24, 87]. Experimental realization of simultaneously negative permittivity and permeability currently relies on resonances in subwavelength unit-cells of metamaterials [15, 25]. However, practical application of such perfect lens is limited due to high loss and small bandwidth of metamaterials.

Negative refraction using PT-symmetric metasurfaces has been proposed to achieve loss-free, all-angle negative refraction and planar focusing [88]. The proposed configuration of such PT-symmetric metasurface is shown in Fig. 6(a). This configuration contains two metasurfaces with gain and loss surface impedances, where both power flow and the phase velocity are directed from the gain surface to the loss surface. Fig. 6(a) shows a clear negative refraction. A backward wave only exists between two surfaces, and the incident wave is totally transmitted through the metasurface without any reflection, despite the presence of loss at the first surface. Ideal focusing of a point source has also been realized by inhomogeneous surface impedances (Fig. 6(a)). More intriguing properties in such negative-refraction PT-symmetric metasurface have been demonstrated [89], including field transformation and aberration-free imaging. Such a configuration of gain/loss metasurface pairs has also been used for invisible cloaks [90].

Angle-independent ideal focusing and volumetric imaging have also been proposed in negative-refraction PT-symmetric metasurface operating at a CPAL point [91]. As shown in Fig. 6(b), the incident field is fully absorbed by loss surface with angle independence, and then the gain surface acts as an emitter to amplify the incident field and reproduce it symmetrically and coherently, leading to ideal focusing of a point source. Due to this mechanism, the ideal focusing is transversely invariant, and the point source can be placed arbitrarily in the object space without any imaging distortion or aberration (Fig. 6(b)). This feature could inspire the development of perfect-focused volume-to-volume imaging technology in the future.

3.6. Surface Waves

Surface wave propagates along an interface of two regions with different permittivity properties. A typical surface mode is surface plasmon polaritons (SPPs) — light-induced oscillations of free electrons on the interface of metal and dielectric surface [92]. Meanwhile, metasurfaces in radiofrequencies support spoof SPPs via architectures such as hole array and comb shape with effective permittivity mimicking the dispersion of metal in optical regime [93, 94]. It is worth mentioning that in most Hermitian settings the unavoidable loss in metasurfaces generally plays a detrimental role. Inspired by the intriguing PT symmetry concept, tailoring the gain-loss interplay in certain parameter regimes of non-Hermitian metasurfaces opens an exciting way towards dynamically manipulating surface waves. For example,
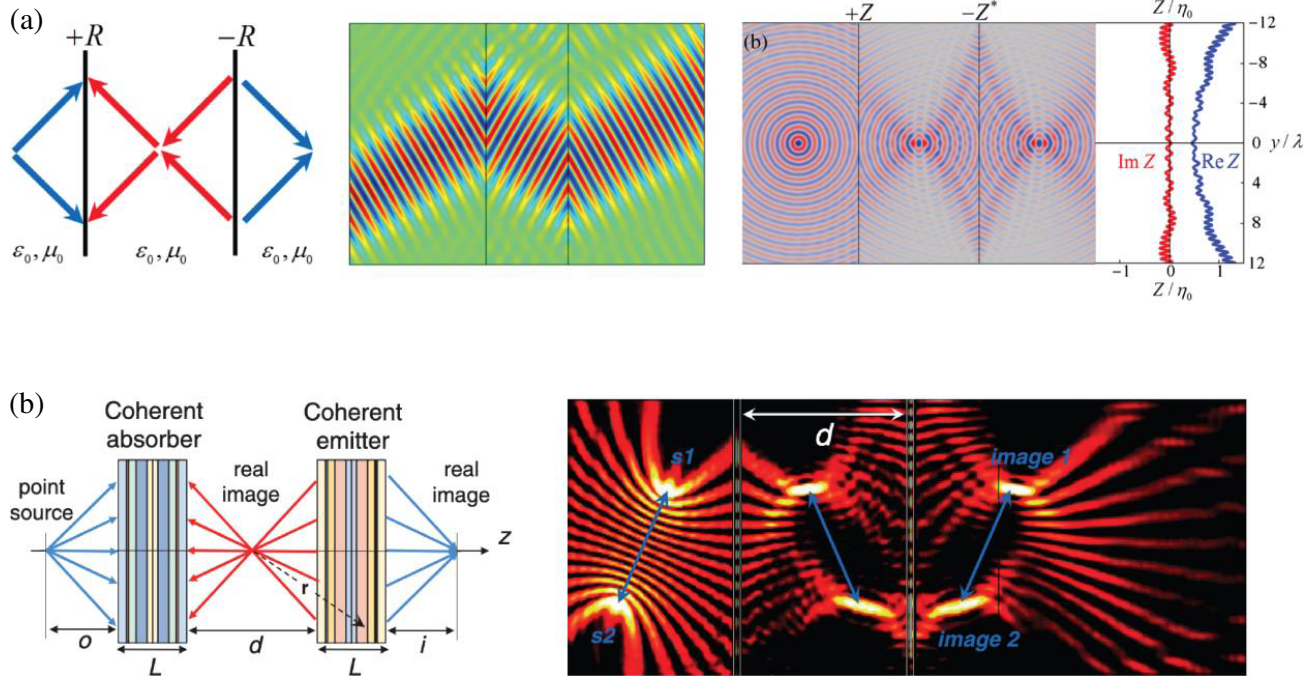
Figure 6. Non-Hermitian metasurfaces for imaging. (a) Left panel: Schematic of non-Hermitian metasurface composed of two surfaces with positive and negative impedances. Middle panel: PT-symmetry-based negative refraction for an obliquely incident Gaussian beam. Right panel: An inhomogeneous surface impedance used for focusing all propagating spatial harmonics of a line source. Reproduced with permission [88]. (b) Left panel: Schematic of nonlocal PT-symmetric metasurface composed of a pair of coherent absorber/emitter. Right panel: Focusing multiple point source by the PT-symmetric metasurface at a CPAL point. Reproduced with permission [91].

Coppolaro et al. explored surface-wave propagation on a non-Hermitian metasurface with extreme anisotropy induced by gain-loss interplay [95]. As shown in Fig. 7(a), this metasurface is composed of 1-D periodical modulation of the real part of surface conductivities between positive and negative values corresponding to loss and gain, respectively. Through the effective-medium theory and full-wave simulations, the numerically computed field maps for the inductive configurations apparently illustrate the canalization phenomena of surface wave, for which the underlying physics completely differs from that in hyperbolic metasurfaces [96, 97].

Line waves, a new type of surface waves localized both out-of-plane and in-plane around the discontinuity with dual (inductive/captive) surface reactances, can propagate unattenuated along a 1-D track [98–100]. The peculiar properties of line waves, such as propagation-dependent polarization, field enhancement and robustness, enable a range of exotic applications in integrated optics and optical sensing. Owning to the intriguing properties of surface waves, a PT-symmetric metasurface, composed of a gain-loss discontinuity characterized by the same reactance but opposite signed resistances, has been put forward to support the line-wave propagation (Fig. 7(b)), which differs from the conventional line waves associated with the duality principle [98]. In particular, it was the first time to modulate the in-plane gain-loss constituents to illustrate the line waves, while in the other scenarios the gain-loss modulations were stacked out-of-plane [38, 91, 101]. The balance between gain and loss gives rise to that line-wave propagation along the gain-loss interface is unattenuated. In addition, spin-momentum locking is one of the intriguing properties of the non-Hermitian line waves, which present the chiral-coupling properties when being excited by circularly polarized sources (Fig. 7(b)). Therefore, the direction of unidirectional propagation is closely relevant to the handedness of circularly polarized sources, which offers future opportunities for applications in valleytronics and quantum optics [102].
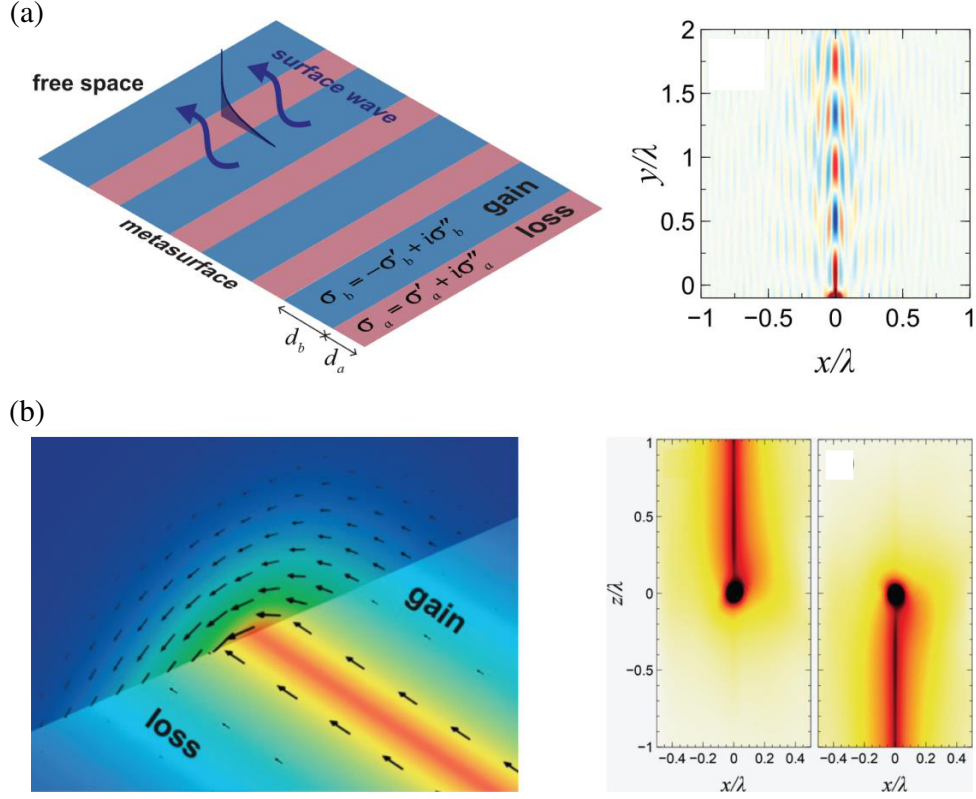
(a)

(b)

Figure 7. Surface waves with non-Hermitian metasurfaces. (a) Left panel: Schematic of non-Hermitian metasurface composed of spatially modulated surface resistance between positive and negative values. Right panel: Numerically computed in-plane field map showing the surface wave and canalization effect. Reproduced with permission [95]. (b) Left panel: Schematic of line wave propagating along a non-Hermitian metasurface with a symmetric discontinuity from gain to loss. Right panel: Numerically computed in-plane electric fields under circularly polarized elementary source of opposite handedness, showing unidirectional propagation along opposite directions. Reproduced with permission [98].

4. CONCLUSION

We have reviewed the recent advances in exception-point and non-Hermitian electromagnetic metasurfaces. Due to mathematical equivalence of Schrödinger equation and Maxwell's theory, the concepts of EP and non-Hermiticity in quantum mechanics can be extended into electromagnetic metasurfaces, which makes metasurfaces as an ideal platform for studying non-Hermitian physics and leverage new functionalities that do not exist in Hermitian counterparts. We have highlighted the milestones of exceptional-point and non-Hermitian metasurfaces with applications ranging from unidirectional propagation, polarization control, diffraction control, ultrasensitive sensing and biosensors, imaging, to surface waves.

Non-Hermiticity paves the way for metasurface design with a new degree of freedom by leveraging gain/loss engineering among unit-cells. Besides of existing design focusing on tuning the radiation losses of coupled resonators, gain-mediated non-Hermitian metasurfaces could lead to stronger field localization and higher quality-factor resonances [103] that are desired for current applications such as absorbers and biosensors [85] although this may increase system's complexity. The integration of gain elements in metasurfaces could be inspired by the studies in non-Hermitian photonics in which the gain is usually provided by ion dopants [5]. In addition, non-Hermitian metasurfaces could be an ideal architecture to study non-Hermitian topological insulators owing to the periodic gain/loss unit-cells in metasurfaces acting as photonic lattice. Topological photonic insulators in Hermitian setting have

attracted much research interest due to their ability to host robust edge states immune to disorder and perturbation, while non-Hermitian topological photonics exhibit a unique feature of non-Hermitian skin effect satisfying non-Hermitian bulk-edge correspondence [104, 105]. Other properties demonstrated in non-Hermitian topological systems, such as topological winding of non-Hermitian band, non-Hermitian topological sensing, and wireless powering, could also be implemented in non-Hermitian metasurfaces for applications that do not exist in the Hermitian setting [106–108].

Reconfigurable metasurfaces with spatially or temporally engineered gain/loss and mode coupling strength offer a promising platform to study time-modulated PT symmetry [109] and the dynamics of non-Hermitian physics [9]. Non-Hermitian metasurfaces with reconfigurability could also realize switchable and adaptive functionalities such as lasing and anti-lasing, absorption and transmission, and multi-polarization converting [39, 44, 110], which could be the key components to be integrated in photonic and quantum systems [111]. Bistable mode switching can also be achieved by metasurfaces satisfying nonlinear PT symmetry, where the bistability happens due to nonadiabatic transitions when the system is encircling an EP [112]. The design of non-Hermitian metasurfaces with reconfigurable gain/loss and dynamic coupling can be enlightened by the strategies in active metasurfaces such as electrical modulation of free carrier density, magneto-optic control, and optical nonlinearity [113].

Non-Hermiticity could be the key to expand the functionalities of metasurfaces. Ultrasensitive measurement is one of the most striking functionalities of non-Hermitian metasurfaces with applications ranging from single particle detection to biomolecular sensing. Given the successful demonstrations of enhanced sensing in optics and radiofrequencies [78, 79], problems remain in these systems such as limited sensitivity due to fabrication imperfection and high intrinsic noise near EP. Potential solutions could be topologically protected EP and exceptional surface that are more robust to undesired perturbations and fabrication errors [114, 115]. Besides, non-Hermitian metasurfaces with the abilities of generating superchiral fields [68] can be applied to sensitive chiral molecule sensing in contrast to weak chirality detection by conventional method of circular dichroism spectroscopy. Such a non-Hermitian metasurface could be an ideal platform to perform surface-enhanced Raman spectroscopy or fluorescence spectroscopy [116]. The superchiral fields generated by non-Hermitian metasurfaces can also enhance the difference of optical forces on chiral molecules, which promises the potential application for chiral molecule sorting [117]. Moreover, non-Hermitian metasurfaces could be utilized for optical bioimaging in which the signal-to-noise performance can be amplified and the optical aberrations can be reduced [91]. Further evaluation will be needed to verify their uses in practical applications ranging from biomedical sensing to optical imaging [118]. Our perspective of non-Hermitian metasurfaces from basic science to potential applications could also provoke the research of metamaterials in other regimes including acoustics, mechanics, and thermotics [119, 120].

ACKNOWLEDGMENT

CONFLICT OF INTEREST

The authors declare no conflict of interest.

REFERENCES

1. Bender, C. M. and S. Boettcher, "Real spectra in non-Hermitian Hamiltonians having PT symmetry," *Physical Review Letters*, Vol. 80, No. 24, 5243, 1998.
2. Miri, M.-A. and A. Alù, "Exceptional points in optics and photonics," *Science*, Vol. 363, No. 6422, 2019.

3. Guo, A., et al., "Observation of PT-symmetry breaking in complex optical potentials," *Physical Review Letters*, Vol. 103, No. 9, 093902, 2009.

4. Bender, C. M., "Making sense of non-Hermitian Hamiltonians," *Reports on Progress in Physics*, Vol. 70, No. 6, 947, 2007.

5. Rüter, C. E., K. G. Makris, R. El-Ganainy, D. N. Christodoulides, M. Segev, and D. Kip, "Observation of parity-time symmetry in optics," *Nature Physics*, Vol. 6, No. 3, 192–195, 2010.

6. Zhao, H. and L. Feng, "Parity-time symmetric photonics," *National Science Review*, Vol. 5, No. 2, 183–199, 2018.

7. Peng, B., et al., "Chiral modes and directional lasing at exceptional points," *Proceedings of the National Academy of Sciences*, Vol. 113, No. 25, 6845–6850, 2016.

8. Feng, L., Z. J. Wong, R.-M. Ma, Y. Wang, and X. Zhang, "Single-mode laser by parity-time symmetry breaking," *Science*, Vol. 346, No. 6212, 972–975, 2014.

9. Xu, H., D. Mason, L. Jiang, and J. Harris, "Topological energy transfer in an optomechanical system with exceptional points," *Nature*, Vol. 537, No. 7618, 80–83, 2016.

10. Regensburger, A., C. Bersch, M.-A. Miri, G. Onishchukov, D. N. Christodoulides, and U. Peschel, "Parity-time synthetic photonic lattices," *Nature*, Vol. 488, No. 7410, 167–171, 2012.

11. Peng, B., et al., "Parity-time-symmetric whispering-gallery microcavities," *Nature Physics*, Vol. 10, No. 5, 394–398, 2014.

12. Zhang, L., S. Mei, K. Huang, and C. W. Qiu, "Advances in full control of electromagnetic waves with metasurfaces," *Advanced Optical Materials*, Vol. 4, No. 6, 818–833, 2016.

13. Ozcan, A. and C.-W. Qiu, *eLight: Enlightening and Exploring Light*, SpringerOpen, 2021.

14. Yu, N., et al., "Light propagation with phase discontinuities: Generalized laws of reflection and refraction," *Science*, Vol. 334, No. 6054, 333–337, 2011.

15. Khorasaninejad, M., W. T. Chen, R. C. Devlin, J. Oh, A. Y. Zhu, and F. Capasso, "Metalenses at visible wavelengths: Diffraction-limited focusing and subwavelength resolution imaging," *Science*, Vol. 352, No. 6290, 1190–1194, 2016.

16. Mehmood, M., et al., "Visible-frequency metasurface for structuring and spatially multiplexing optical vortices," *Advanced Materials*, Vol. 28, No. 13, 2533–2539, 2016.

17. Li, H.-P., G.-M. Wang, J.-G. Liang, and X.-J. Gao, "Wideband multifunctional metasurface for polarization conversion and gain enhancement," *Progress In Electromagnetics Research*, Vol. 155, 115–125, 2016.

18. Lin, B.-Q., J. Guo, Y. Wang, Z. Wang, B. Huang, and X. Liu, "A wide-angle and wide-band circular polarizer using a bi-layer metasurface," *Progress In Electromagnetics Research*, Vol. 161, 125–133, 2018.

19. Schurig, D., et al., "Metamaterial electromagnetic cloak at microwave frequencies," *Science*, Vol. 314, No. 5801, 977–980, 2006.

20. Landy, N. I., S. Sajuyigbe, J. J. Mock, D. R. Smith, and W. J. Padilla, "Perfect metamaterial absorber," *Physical Review Letters*, Vol. 100, No. 20, 207402, 2008.

21. Huang, L., et al., "Three-dimensional optical holography using a plasmonic metasurface," *Nature Communications*, Vol. 4, No. 1, 1–8, 2013.

22. Chen, J., Q. Cheng, J. Zhao, D. S. Dong, and T.-J. Cui, "Reduction of radar cross section based on a metasurface," *Progress In Electromagnetics Research*, Vol. 146, 71–76, 2014.

23. Hsu, L. Y., T. Lepetit, and B. Kanté, "Extremely thin dielectric metasurface for carpet cloaking," *Progress In Electromagnetics Research*, Vol. 152, 33–40, 2015.

24. Pendry, J. B., "Negative refraction makes a perfect lens," *Physical Review Letters*, Vol. 85, No. 18, 3966, 2000.

25. Shelby, R. A., D. R. Smith, and S. Schultz, "Experimental verification of a negative index of refraction," *Science*, Vol. 292, No. 5514, 77–79, 2001.

26. Feng, L., R. El-Ganainy, and L. Ge, "Non-Hermitian photonics based on parity-time symmetry," *Nature Photonics*, Vol. 11, No. 12, 752–762, 2017.

27. Shankar, R., *Principles of Quantum Mechanics*, Springer Science & Business Media, 2012.

28. Mostafazadeh, A., "Pseudo-Hermiticity versus PT symmetry: The necessary condition for the reality of the spectrum of a non-Hermitian Hamiltonian," *Journal of Mathematical Physics*, Vol. 43, No. 1, 205–214, 2002.

29. Longhi, S., "Quantum-optical analogies using photonic structures," *Laser & Photonics Reviews*, Vol. 3, No. 3, 243–261, 2009.

30. Klaiman, S., U. Günther, and N. Moiseyev, "Visualization of branch points in p t-symmetric waveguides," *Physical Review Letters*, Vol. 101, No. 8, 080402, 2008.

31. Haus, H. A. and W. Huang, "Coupled-mode theory," *Proceedings of the IEEE*, Vol. 79, No. 10, 1505–1518, 1991.

32. Ghoshroy, A., Ş. K. Özdemir, and D. Ö. Güney, "Loss compensation in metamaterials and plasmonics with virtual gain," *Optical Materials Express*, Vol. 10, No. 8, 1862–1880, 2020.

33. Gu, X., et al., "Unidirectional reflectionless propagation in a non-ideal parity-time metasurface based on far field coupling," *Optics Express*, Vol. 25, No. 10, 11778–11787, 2017.

34. Wang, D., et al., "Superconductive PT-symmetry phase transition in metasurfaces," *Applied Physics Letters*, Vol. 110, No. 2, 021104, 2017.

35. Sakhdari, M., M. Farhat, and P.-Y. Chen, "PT-symmetric metasurfaces: Wave manipulation and sensing using singular points," *New Journal of Physics*, Vol. 19, No. 6, 065002, 2017.

36. Feng, L., et al., "Experimental demonstration of a unidirectional reflectionless parity-time metamaterial at optical frequencies," *Nature Materials*, Vol. 12, No. 2, 108–113, 2013.

37. Ge, L., Y. Chong, and A. D. Stone, "Conservation relations and anisotropic transmission resonances in one-dimensional PT-symmetric photonic heterostructures," *Physical Review A*, Vol. 85, No. 2, 023802, 2012.

38. Chen, P.-Y. and J. Jung, "P T symmetry and singularity-enhanced sensing based on photoexcited graphene metasurfaces," *Physical Review Applied*, Vol. 5, No. 6, 064018, 2016.

39. Lawrence, M., et al., "Manifestation of PT symmetry breaking in polarization space with terahertz metasurfaces," *Physical Review Letters*, Vol. 113, No. 9, 093901, 2014.

40. Droulias, S., I. Katsantonis, M. Kafesaki, C. M. Soukoulis, and E. N. Economou, "Chiral metamaterials with PT symmetry and beyond," *Physical Review Letters*, Vol. 122, No. 21, 213201, 2019.

41. Kang, M., J. Chen, and Y. Chong, "Chiral exceptional points in metasurfaces," *Physical Review A*, Vol. 94, No. 3, 033834, 2016.

42. Huang, Y., Y. Shen, C. Min, S. Fan, and G. Veronis, "Unidirectional reflectionless light propagation at exceptional points," *Nanophotonics*, Vol. 6, No. 5, 977–996, 2017.

43. Hahn, C., S. H. Song, C. H. Oh, and P. Berini, "Single-mode lasers and parity-time symmetry broken gratings based on active dielectric-loaded long-range surface plasmon polariton waveguides," *Optics Express*, Vol. 23, No. 15, 19922–19931, 2015.

44. Lin, Z., H. Ramezani, T. Eichelkraut, T. Kottos, H. Cao, and D. N. Christodoulides, "Unidirectional invisibility induced by P T-symmetric periodic structures," *Physical Review Letters*, Vol. 106, No. 21, 213901, 2011.

45. Jia, Y., Y. Yan, S. V. Kesava, E. D. Gomez, and N. C. Giebink, "Passive parity-time symmetry in organic thin film waveguides," *ACS Photonics*, Vol. 2, No. 2, 319–325, 2015.

46. Feng, L., et al., "Demonstration of a large-scale optical exceptional point structure," *Optics Express*, Vol. 22, No. 2, 1760–1767, 2014.

47. Huang, Y., C. Min, and G. Veronis, "Broadband near total light absorption in non-PT-symmetric waveguide-cavity systems," *Optics Express*, Vol. 24, No. 19, 22219–22231, 2016.

48. Huang, Y., G. Veronis, and C. Min, "Unidirectional reflectionless propagation in plasmonic waveguide-cavity systems at exceptional points," *Optics Express*, Vol. 23, No. 23, 29882–29895, 2015.

49. Min, S. Y., J. Y. Kim, S. Yu, S. G. Menabde, and M. S. Jang, "Exceptional points in plasmonic waveguides do not require gain or loss," *Physical Review Applied*, Vol. 14, No. 5, 054041, 2020.

50. Wang, C., et al., "Electromagnetically induced transparency at a chiral exceptional point," *Nature Physics*, Vol. 16, No. 3, 334–340, 2020.

51. Chen, H.-Z., et al., "Revealing the missing dimension at an exceptional point," *Nature Physics*, Vol. 16, No. 5, 571–578, 2020.

52. Huang, X., C. Lu, C. Liang, H. Tao, and Y.-C. Liu, "Loss-induced nonreciprocity," *Light: Science & Applications*, Vol. 10, No. 1, 1–8, 2021.

53. Peng, B., et al., "Loss-induced suppression and revival of lasing," *Science*, Vol. 346, No. 6207, 328–332, 2014.

54. Dong, S., et al., "Loss-assisted metasurface at an exceptional point," *ACS Photonics*, 2020.

55. Cao, G., et al., "Fano resonance in artificial photonic molecules," *Advanced Optical Materials*, Vol. 8, No. 10, 1902153, 2020.

56. Chen, J., et al., "Manipulating mode degeneracy for tunable spectral characteristics in multi-microcavity photonic molecules," *Optics Express*, Vol. 29, No. 7, 11181–11193, 2021.

57. Deng, Y., G. Cao, H. Yang, G. Li, X. Chen, and W. Lu, "Tunable and high-sensitivity sensing based on Fano resonance with coupled plasmonic cavities," *Scientific Reports*, Vol. 7, No. 1, 1–8, 2017.

58. Lin, G., et al., "Ultra-compact high-sensitivity plasmonic sensor based on Fano resonance with symmetry breaking ring cavity," *Optics Express*, Vol. 27, No. 23, 33359–33368, 2019.

59. Liu, Q., B. Wang, S. Ke, H. Long, K. Wang, and P. Lu, "Exceptional points in Fano-resonant graphene metamaterials," *Optics Express*, Vol. 25, No. 7, 7203–7212, 2017.

60. Zhao, Y. and A. Alù, "Manipulating light polarization with ultrathin plasmonic metasurfaces," *Physical Review B*, Vol. 84, No. 20, 205428, 2011.

61. Yang, H., G. Cao, X. Shang, T. Li, G. Yang, and G. Li, "Anisotropic metasurfaces for efficient polarization independent wavefront steering," *Journal of Physics D: Applied Physics*, Vol. 53, No. 4, 045104, 2019.

62. Ou, K., et al., "High efficiency focusing vortex generation and detection with polarization-insensitive dielectric metasurfaces," *Nanoscale*, Vol. 10, No. 40, 19154–19161, 2018.

63. Yang, H., et al., "Polarization-independent metalens constructed of antennas without rotational invariance," *Optics Letters*, Vol. 42, No. 19, 3996–3999, 2017.

64. Cao, T., Y. Cao, and L. Fang, "Reconfigurable parity-time symmetry transition in phase change metamaterials," *Nanoscale*, Vol. 11, No. 34, 15828–15835, 2019.

65. Park, S. H., et al., "Observation of an exceptional point in a non-Hermitian metasurface," *Nanophotonics*, Vol. 9, No. 5, 1031–1039, 2020.

66. Dembowski, C., et al., "Experimental observation of the topological structure of exceptional points," *Physical Review Letters*, Vol. 86, No. 5, 787, 2001.

67. Doppler, J., et al., "Dynamically encircling an exceptional point for asymmetric mode switching," *Nature*, Vol. 537, No. 7618, 76–79, 2016.

68. Wu, T., et al., "Vector exceptional points with strong superchiral fields," *Physical Review Letters*, Vol. 124, No. 8, 083901, 2020.

69. Li, J., J. Fu, Q. Liao, and S. Ke, "Exceptional points in chiral metasurface based on graphene strip arrays," *JOSA B*, Vol. 36, No. 9, 2492–2498, 2019.

70. Leung, H. M., et al., "Exceptional point-based plasmonic metasurfaces for vortex beam generation," *Optics Express*, Vol. 28, No. 1, 503–510, 2020.

71. Kang, M., W. Zhu, and I. D. Rukhlenko, "Experimental observation of the topological structure of exceptional points in an ultrathin hybridized metamaterial," *Physical Review A*, Vol. 96, No. 6, 063823, 2017.

72. Li, S., et al., "Exceptional point in a metal-graphene hybrid metasurface with tunable asymmetric loss," *Optics Express*, Vol. 28, No. 14, 20083–20094, 2020.

73. Chen, H.-T., A. J. Taylor, and N. Yu, "A review of metasurfaces: Physics and applications," *Reports on Progress in Physics*, Vol. 79, No. 7, 076401, 2016.

74. Jahani, S. and Z. Jacob, "All-dielectric metamaterials," *Nature Nanotechnology*, Vol. 11, No. 1, 23–36, 2016.

75. Nye, N., A. Halawany, C. Markos, M. Khajavikhan, and D. Christodoulides, "Flexible PT-symmetric optical metasurfaces," *Physical Review Applied*, Vol. 13, No. 6, 064005, 2020.

76. Zhao, B., L.-S. Sun, and J. Chen, "Hybrid parity-time modulation phase and geometric phase in metasurfaces," *Optics Express*, Vol. 28, No. 20, 28896–28905, 2020.

77. Wiersig, J., "Sensors operating at exceptional points: General theory," *Physical Review A*, Vol. 93, No. 3, 033809, 2016.

78. W. Chen, Ş. K. Özdemir, G. Zhao, J. Wiersig, and L. Yang, "Exceptional points enhance sensing in an optical microcavity," *Nature*, Vol. 548, No. 7666, 192–196, 2017.

79. Dong, Z., Z. Li, F. Yang, C.-W. Qiu, and J. S. Ho, "Sensitive readout of implantable microsensors using a wireless system locked to an exceptional point," *Nature Electronics*, Vol. 2, No. 8, 335–342, 2019.

80. Jin, B., et al., "High-performance terahertz sensing at exceptional points in a bilayer structure," *Advanced Theory and Simulations*, Vol. 1, No. 9, 1800070, 2018.

81. Ma, Y., et al., "Semiconductor-based plasmonic interferometers for ultrasensitive sensing in a terahertz regime," *Optics Letters*, Vol. 42, No. 12, 2338–2341, 2017.

82. Grognot, M. and G. Gallot, "Quantitative measurement of permeabilization of living cells by terahertz attenuated total reflection," *Applied Physics Letters*, Vol. 107, No. 10, 103702, 2015.

83. Farhat, M., M. Yang, Z. Ye, and P.-Y. Chen, "PT-symmetric absorber-laser enables electromagnetic sensors with unprecedented sensitivity," *ACS Photonics*, Vol. 7, No. 8, 2080–2088, 2020.

84. Xiao, S., J. Gear, S. Rotter, and J. Li, "Effective PT-symmetric metasurfaces for subwavelength amplified sensing," *New Journal of Physics*, Vol. 18, No. 8, 085004, 2016.

85. Park, J.-H., et al., "Symmetry-breaking-induced plasmonic exceptional points and nanoscale sensing," *Nature Physics*, Vol. 16, No. 4, 462–468, 2020.

86. Mortensen, N. A., P. Gonçalves, M. Khajavikhan, D. N. Christodoulides, C. Tserkezis, and C. Wolff, "Fluctuations and noise-limited sensing near the exceptional point of parity-time-symmetric resonator systems," *Optica*, Vol. 5, No. 10, 1342–1346, 2018.

87. Veselago, V. G., "The electrodynamics of substances with simultaneously negative values of Img Align = Absmiddle Alt = ϵ Eps/Img and μ," *Physics-Uspekhi*, Vol. 10, No. 4, 509–514, 1968.

88. Fleury, R., D. L. Sounas, and A. Alú, "Negative refraction and planar focusing based on parity-time symmetric metasurfaces," *Physical Review Letters*, Vol. 113, No. 2, 023903, 2014.

89. Valagiannopoulos, C., F. Monticone, and A. Alú, "PT-symmetric planar devices for field transformation and imaging," *Journal of Optics*, Vol. 18, No. 4, 044028, 2016.

90. Sounas, D. L., R. Fleury, and A. Alù, "Unidirectional cloaking based on metasurfaces with balanced loss and gain," *Physical Review Applied*, Vol. 4, No. 1, 014005, 2015.

91. Monticone, F., C. A. Valagiannopoulos, and A. Alù, "Parity-time symmetric nonlocal metasurfaces: All-angle negative refraction and volumetric imaging," *Physical Review X*, Vol. 6, No. 4, 041018, 2016.

92. Barnes, W. L., A. Dereux, and T. W. Ebbesen, "Surface plasmon subwavelength optics," *Nature*, Vol. 424, No. 6950, 824–830, 2003.

93. Tian, X., et al., "Wireless body sensor networks based on metamaterial textiles," *Nature Electronics*, Vol. 2, No. 6, 243–251, 2019.

94. Pendry, J., L. Martin-Moreno, and F. Garcia-Vidal, "Mimicking surface plasmons with structured surfaces," *Science*, Vol. 305, No. 5685, 847–848, 2004.

95. Coppolaro, M., M. Moccia, G. Castaldi, A. Alù, and V. Galdi, "Surface-wave propagation on non-hermitian metasurfaces with extreme anisotropy," *IEEE Transactions on Microwave Theory and Techniques*, Vol. 69, No. 4, 2060–2071, 2021.

96. Gomez-Diaz, J. S., M. Tymchenko, and A. Alù, "Hyperbolic plasmons and topological transitions over uniaxial metasurfaces," *Physical Review Letters*, Vol. 114, No. 23, 233901, 2015.

97. Gomez-Diaz, J., M. Tymchenko, and A. Alù, "Hyperbolic metasurfaces: Surface plasmons, light-matter interactions, and physical implementation using graphene strips," *Optical Materials Express*, Vol. 5, No. 10, 2313–2329, 2015.

98. Moccia, M., G. Castaldi, A. Alù, and V. Galdi, "Line waves in non-hermitian metasurfaces," *ACS Photonics*, Vol. 7, No. 8, 2064–2072, 2020.

99. Horsley, S. and I. R. Hooper, "One dimensional electromagnetic waves on flat surfaces," *Journal of Physics D: Applied Physics*, Vol. 47, No. 43, 435103, 2014.

100. Dia'aaldin, J. B. and D. F. Sievenpiper, "Guiding waves along an infinitesimal line between impedance surfaces," *Physical Review Letters*, Vol. 119, No. 10, 106802, 2017.

101. Sakhdari, M., N. M. Estakhri, H. Bagci, and P.-Y. Chen, "Low-threshold lasing and coherent perfect absorption in generalized PT-symmetric optical structures," *Physical Review Applied*, Vol. 10, No. 2, 024030, 2018.

102. Lodahl, P., et al., "Chiral quantum optics," *Nature*, Vol. 541, No. 7638, 473–480, 2017.

103. Zhang, Y.-R., J.-Q. Yuan, Z.-Z. Zhang, M. Kang, and J. Chen, "Exceptional singular resonance in gain mediated metamaterials," *Optics Express*, Vol. 27, No. 5, 6240–6248, 2019.

104. Xiao, L., et al., "Non-Hermitian bulk-boundary correspondence in quantum dynamics," *Nature Physics*, 1–6, 2020.

105. Okuma, N., K. Kawabata, K. Shiozaki, and M. Sato, "Topological origin of non-Hermitian skin effects," *Physical Review Letters*, Vol. 124, No. 8, 086801, 2020.

106. Wang, K., A. Dutt, K. Y. Yang, C. C. Wojcik, J. Vučković, and S. Fan, "Generating arbitrary topological windings of a non-Hermitian band," *Science*, Vol. 371, No. 6535, 1240–1245, 2021.

107. Budich, J. C. and E. J. Bergholtz, "Non-Hermitian topological sensors," *Physical Review Letters*, Vol. 125, No. 18, 180403, 2020.

108. Song, J., et al., "Wireless power transfer via topological modes in dimer chains," *Physical Review Applied*, Vol. 15, No. 1, 014009, 2021.

109. Li, H., H. Moussa, D. Sounas, and A. Alù, "Parity-time symmetry based on time modulation," *Physical Review Applied*, Vol. 14, No. 3, 031002, 2020.

110. Wong, Z. J., et al., "Lasing and anti-lasing in a single cavity," *Nature Photonics*, Vol. 10, No. 12, 796–801, 2016.

111. Wang, J., F. Sciarrino, A. Laing, and M. G. Thompson, "Integrated photonic quantum technologies," *Nature Photonics*, Vol. 14, No. 5, 273–284, 2020.

112. Wang, H., S. Assawaworrarit, and S. Fan, "Dynamics for encircling an exceptional point in a nonlinear non-Hermitian system," *Optics Letters*, Vol. 44, No. 3, 638–641, 2019.

113. Shaltout, A. M., V. M. Shalaev, and M. L. Brongersma, "Spatiotemporal light control with active metasurfaces," *Science*, Vol. 364, No. 6441, 2019.

114. Zhong, Q., J. Ren, M. Khajavikhan, D. N. Christodoulides, Ş. Özdemir, and R. El-Ganainy, "Sensing with exceptional surfaces in order to combine sensitivity with robustness," *Physical Review Letters*, Vol. 122, No. 15, 153902, 2019.

115. Gu, Z., et al., "Topologically protected exceptional point with local non-hermitian modulation in an acoustic crystal," *Physical Review Applied*, Vol. 15, No. 1, 014025, 2021.

116. Moskovits, M., "Surface-enhanced spectroscopy," *Reviews of Modern Physics*, Vol. 57, No. 3, 783, 1985.

117. Alaee, R., B. Gurlek, J. Christensen, and M. Kadic, "Optical force rectifiers based on PT-symmetric metasurfaces," *Physical Review B*, Vol. 97, No. 19, 195420, 2018.

118. Li, Z., X. Tian, C.-W. Qiu, and J. S. Ho, "Metasurfaces for bioelectronics and healthcare," *Nature Electronics*, 1–10, 2021.

119. Barchiesi, E., M. Spagnuolo, and L. Placidi, "Mechanical metamaterials: A state of the art," *Mathematics and Mechanics of Solids*, Vol. 24, No. 1, 212–234, 2019.

120. Li, Y., et al., "Transforming heat transfer with thermal metamaterials and devices," *Nature Reviews Materials*, 1–20, 2021.